



HAL
open science

Heat Transfer in Turbulent Rayleigh-Bénard Convection below the Ultimate Regime

Philippe-Emmanuel Roche, Bernard Castaing, Benoît Chabaud, B. Hébral

► **To cite this version:**

Philippe-Emmanuel Roche, Bernard Castaing, Benoît Chabaud, B. Hébral. Heat Transfer in Turbulent Rayleigh-Bénard Convection below the Ultimate Regime. 2003. hal-00000512v2

HAL Id: hal-00000512

<https://hal.science/hal-00000512v2>

Preprint submitted on 10 Aug 2003 (v2), last revised 14 Oct 2003 (v3)

HAL is a multi-disciplinary open access archive for the deposit and dissemination of scientific research documents, whether they are published or not. The documents may come from teaching and research institutions in France or abroad, or from public or private research centers.

L'archive ouverte pluridisciplinaire **HAL**, est destinée au dépôt et à la diffusion de documents scientifiques de niveau recherche, publiés ou non, émanant des établissements d'enseignement et de recherche français ou étrangers, des laboratoires publics ou privés.



Heat transfer in turbulent Rayleigh-Bénard convection below the ultimate regime

P.-E. Roche, B. Castaing*, B. Chabaud and B. Hébral

*Centre de Recherches sur les Très Basses Températures
Laboratoire du CNRS, associé à l'Université Joseph Fourier
25 avenue des Martyrs, 38042 Grenoble Cedex 9, France*

**Ecole Normale Supérieure de Lyon
46 allée d'Italie, 69364 Lyon Cedex 07, France*

Keywords: Rayleigh-Bénard, Convection, Turbulence, Turbulent, Heat transfer, Nusselt, Helium, He properties, thermal expansion, sidewall, bimodality, Prandtl, Rayleigh

PACS: 47.27.Te Convection and heat transfer , 44.25.+f Natural convection , 67.90.+z Other topics in quantum fluids and solids; liquid and solid helium

Abstract

A Rayleigh-Bénard cell has been designed to explore the Prandtl (Pr) dependence of turbulent convection in the cross-over range $0.7 < Pr < 21$ and for the full range of soft and hard turbulences, up to Rayleigh number $Ra \simeq 10^{11}$. The set-up benefits from the favourable characteristics of cryogenic helium-4 in fluid mechanics, in-situ fluid property measurements and special care on thermometry and calorimetric instrumentation. The effective heat transfer $Nu(Ra, Pr)$ has been measured with unprecedented accuracy for cryogenic convection experiments. Spin-off of this study include improved fits of helium thermodynamics and viscosity properties. Three main results were found. First the $Nu(Ra)$ dependence exhibits a bimodality of the flow with 4–7% difference in Nu for given Ra and Pr . Second, a systematic study of the side-wall influence reveals an significant bias on the heat transfer. Third, the $Nu(Pr)$ dependence is very small or null : the absolute value of the average logarithmic slope $(d \ln Nu / d \ln Pr)_{Ra}$ is smaller than 0.03 in our range of Pr .

1 Introduction

Static equilibrium in a column of fluid corresponds to a balance between many parameters such as the weight, the pressure gradient, the temperature difference, etc. The occurrence of a small local perturbation can initiate a global convective motion. Rayleigh-Bénard convection is a reference configuration for convection studies: a fluid cylinder (height h , section S) located between two horizontal plates is submitted to a temperature difference ΔT between the plates. In our case the upper plate is maintained at constant temperature

and ΔT results from a constant heat flux \dot{Q} applied at the bottom plate. For high enough ΔT the convective flow turns into a turbulent regime.

For a given fluid at mean temperature T with a mass density ρ , and for fixed geometrical conditions, the convective flow is characterized by one single parameter ΔT or the dimensionless Rayleigh number defined as: $Ra = \frac{\alpha g h^3 \Delta T}{\nu \kappa}$. In this expression:

- ν is the kinematic viscosity, κ the thermal diffusivity ; their ratio is the Prandtl number: $Pr = \nu/\kappa$,
- α is the constant-pressure thermal expansion coefficient,
- g is the gravity acceleration.

The Nusselt number gives the apparent thermal conductivity in the cell: $Nu = \frac{\dot{Q}h}{\lambda S \Delta T}$ (λ is the fluid thermal conductivity). In a given cell, Nu should depend only of Ra and Pr .

The unique properties of cryogenic ^4He allow to control high Rayleigh numbers[1, 2, 3, 4]. These were used in Grenoble[3, 5] to reach Ra higher than 10^{14} in high cells (aspect ratio 1/2, $h = 20$ cm) : in such conditions we observed for the first time the so-called *ultimate regime* predicted by Kraichnan[6] forty years ago.

Helium gives also the opportunity to easily vary the Prandtl number on an unusual range. We have done a specific study of the Pr variation effect in a small size cell (called the mini-cell, aspect ratio 1/2, $h = 2$ cm), for $3.10^6 < Ra < 10^{11}$ corresponding to the soft and hard turbulence regimes where experimentally controlled Pr can be achieved independently of Ra (the lowest explored Ra in this work is below 10^4 and the convection threshold was found to be the same as in the large cells, around 4.10^4). This Ra range fully covers the turbulent regimes preceding the transition towards the ultimate regime and allows a comparison with other experiments using various fluids, and also several models.

Iso- Ra_{max} curves have been calculated at various pressures and temperatures for the mini-cell and for the maximum temperature difference ΔT_{max} compatible with a Boussinesq criterion[7], here defined as: $\alpha \Delta T < 20\%$. This criterion is also respected in the experimental data. In density-temperature coordinates iso- Ra_{max} curves are shown on figures 1-a and reffig:RaMaxi-b as the thick full lines. The divergence of $\frac{1}{\nu\kappa}$, easily accessible in ^4He (2.2 bars, 5.2 K) is clearly illustrated by the extremely high Ra which can be achieved in reasonable experimental conditions ($\Delta T > 1$ mK). The small lines on figure 1-a correspond to isochores.

Similarly iso- Pr are shown on figure 2. In the large cells[3, 5], the Pr variation is only obtained for Ra above 10^{10} . Clear understanding of the Pr variation is difficult in these cells due to the occurrence of the ultimate regime. With cell dimensions divided by ten, the Pr variation is already observable around $Ra = 10^7$. The points represent the various experimental conditions selected for our mini-cell experiment, which will be described later.

It is worth noticing that the divergence in Ra_{max} is due to: $\frac{1}{\nu\kappa} = \frac{C_p \rho^2}{\eta \lambda}$, η being the fluid viscosity and C_p the specific heat at constant pressure. The Prandtl number varies as: $Pr = \frac{C_p \eta}{\rho \kappa}$. The C_p divergence appears far away from the critical point and gives a long range effect to the rapid variation of Ra and Pr . For each experimental point on figure 2, ΔT has been widely varied up to three decades. This is the largest excursion ever achieved in Rayleigh-Bénard experiments under the Boussinesq condition. This gives access to power law exponent Nu vs. Ra at constant Pr and independently of the fluid properties knowledge. However these properties have to be precisely determined for the Nu vs. Pr dependence studies.

This experiment has been designed to study the Prandtl dependence in the cross-over range $0.7 < Pr < 21$ and for a large excursion of Ra numbers. The thermal control and measurement accuracy are unprecedented in cryogenics convection experiments. It reveals two unexpected effects. This paper gives a detailed description of the apparatus (section

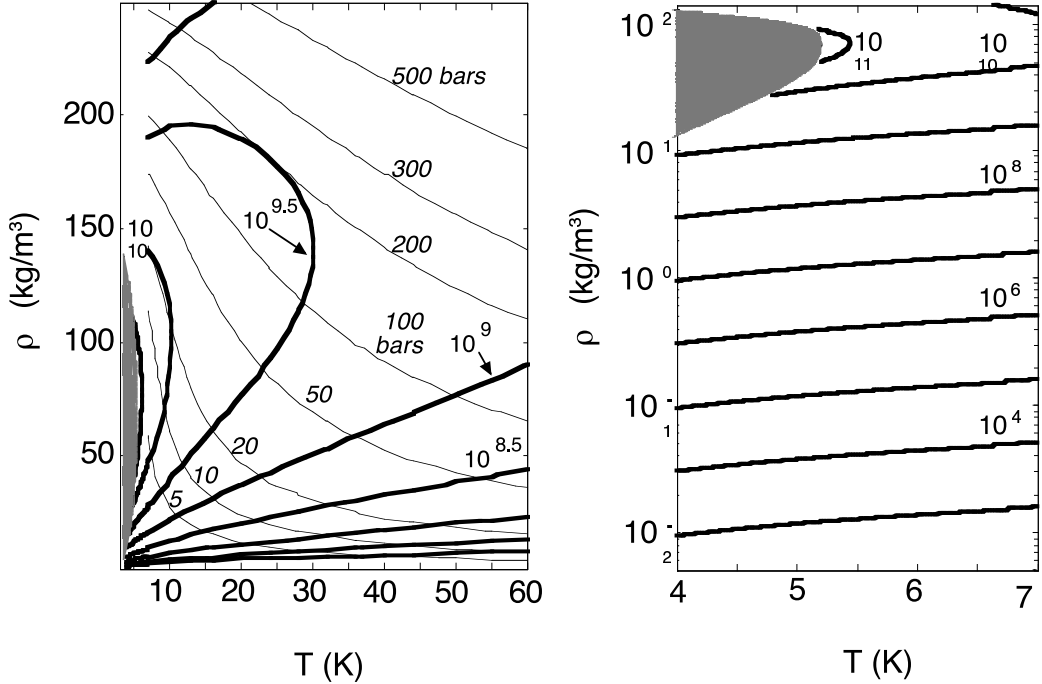


Figure 1: a-Isochores and iso- Ra_{max} in the density-temperature plane. b- Semi log enlargement of subplot a, corresponding to the experiments described in the text. The maximum Ra achieved within Boussinesq conditions in the 2 cm high cell is 10^{11} . The dark area corresponds to the 2-phases region.

2) and improvements of ${}^4\text{He}$ properties fits (section 3). In section 4, we recall the three main results : the bimodality of the flow, the side-wall effect and the Prandtl number dependence. Section 5 proposes some perspectives for convection studies.

2 Instrumentation

2.1 The Rayleigh-Bénard cell design

The experimental set-up, presented on figure 3, is placed under high cryogenic vacuum. The 1/2 aspect ratio mini-cell ($h = 2\text{ cm}$), is also shown on figure 4. The stainless-steel cylindrical wall is 0.25 mm thick. It can hold pressures up to several tens of bars. The upper plate is part of a main Cu flange which ensures the thermal link to the liquid He bath, through a calibrated brass plate and a high conductivity Cu post[8, 9]. The lower plate is also made of copper. In such a cryogenic helium/copper set-up and for the Ra numbers of this study, the plate properties (finite conductivity and heat capacity) don't alter the dynamical formation of the coherent structures (plumes,...) [10, 11].

Special care has been taken during the cell assembly. The rugosity of the plate surfaces in contact with the fluid is estimated less than $2\ \mu\text{m}$. The silver soldering of the wall and the copper rings ensures the connection to the plates. For all the cells developed in our group, the side wall design is chosen in order to have a perfect cylinder on all the active length of the cell[8, 9]. The plates parallelism is guaranteed by special machining procedure performed *after* the silver soldering: the distance between plates is $19.99 \pm 0.02\ \text{mm}$.

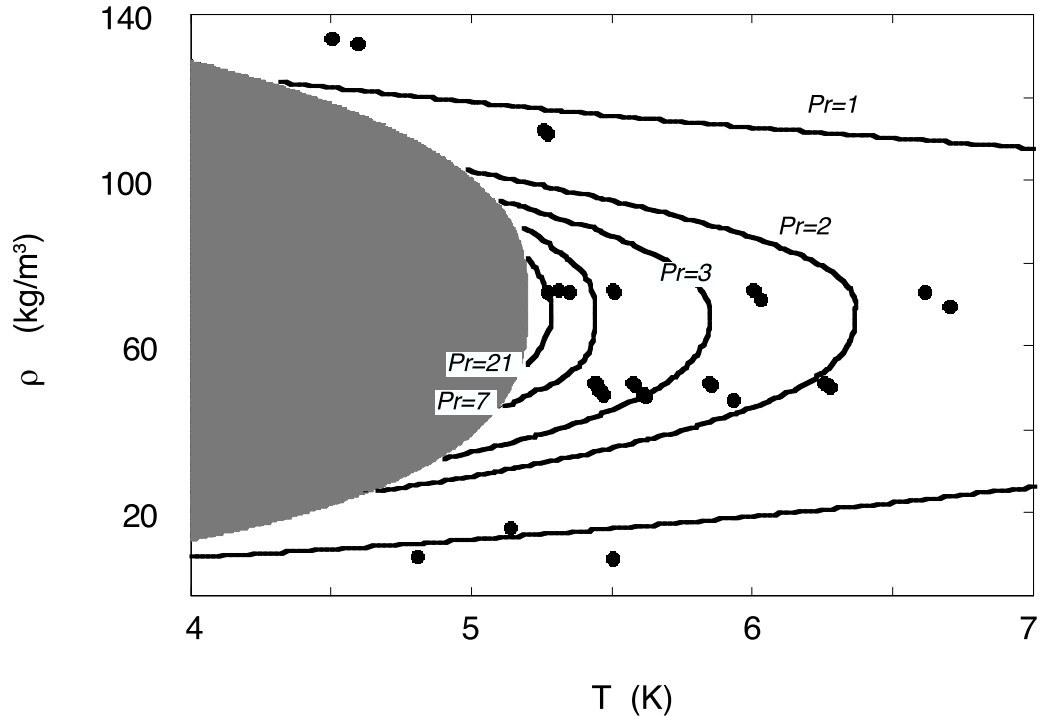


Figure 2: Iso- Pr curves and experimental points explored in this work. The dark area corresponds to the 2-phases region.

The cell is filled through a capillary closed with a cold needle valve located in the main helium bath. This capillary is connected in series with a capacitance cell, that will be further described, and the Rayleigh-Bénard cell.

2.2 Experimental procedure

Each cell plate has two Ge resistors from the same batch with close resistance values and temperature dependence. The upper flange is temperature regulated with a PID analog regulator with a fifth Ge resistor. The temperature difference ΔT between the plates in the Rayleigh-Bénard cell is determined from the measurement of the ratio of two Ge resistors using a specially designed resistance ratio bridge operating at 30 Hz with 1 μA current amplitude. The resistance ratio variation with and without heating gives ΔT through the calibration of the resistors and the additional measurement of the upper plate temperature. This procedure is valid even for ΔT larger than 1 K, as checked with the direct temperature measurement of each plate. The ratio without heating (zero ΔT) is monitored during twelve hours before and after each measurement cycle. In less than one hour the equilibrium value is obtained, except for the data close to the critical point: in such conditions the thermal diffusion time diverges and the used zero ΔT is the one obtained at a lower density.

A ratio variation of 10^{-5} at 5 K corresponds to 25 μK for ΔT . The stability of the set-up and electronic apparatus is better than 30 μK over 12 h. The radiation heat losses are estimated to be around 10 nW which gives typically 50 μK for ΔT . This is of the order of the adiabatic gradient temperature difference[7, 8] in the 2 cm high cell, this effect limiting the smallest achievable ΔT . More than 3 decades of variation of ΔT have been achieved for given mean temperature and density, from below the convection onset

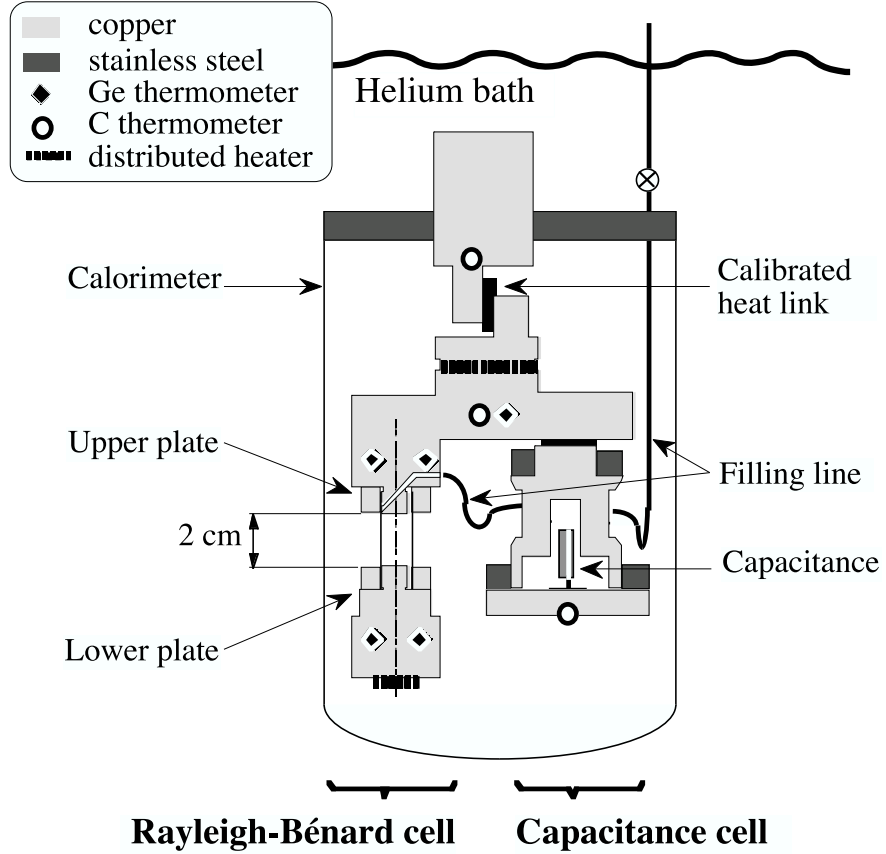


Figure 3: Scheme of the experimental set-up.

up to the turbulent regimes. In large cells, an original thermocouple technique is more appropriate than a resistance bridge: the ΔT zeroing procedure is not compatible with the large thermal relaxation times.

A four wires voltage standard (Electronics Development Corporation) gives a constant heating power to the lower plate. In order to limit local overheating the heater is distributed on the surface. All the copper pieces are made out of a commercial non-annealed Cu, which was characterized in another experiment: its thermal conductivity is around 400 W/m.K . We have measured the wall thermal conductance between 4.5 and 6 K. For cross-validation, two measurements have been done with an empty cell and with helium at 80 g/cm^3 . After subtraction of the diffusive helium contribution both results agree within 2.5%: in this difference 2% are explained by the cell design[9]. This side-wall contribution is described by: $-40.1 + 44.75.T$ in $\mu\text{W/K}$ including the conductance of the copper heating wires ($33 \mu\text{W/K}$ at 4.5 K with 20% uncertainty) going to the lower plate. The lower plate heat capacity, as measured by a relaxation method, is 73 mJ/K including addenda (Ge resistor holders and copper ring). The brass plate heat leak has a measured resistance of 53 K/W at 4.3 K.

2.3 Densitometry

In order to determine the Ra and Nu with an absolute resolution of a few percent, a density precision of 1%, at least, is needed. The dead volume coming from the filling capillary

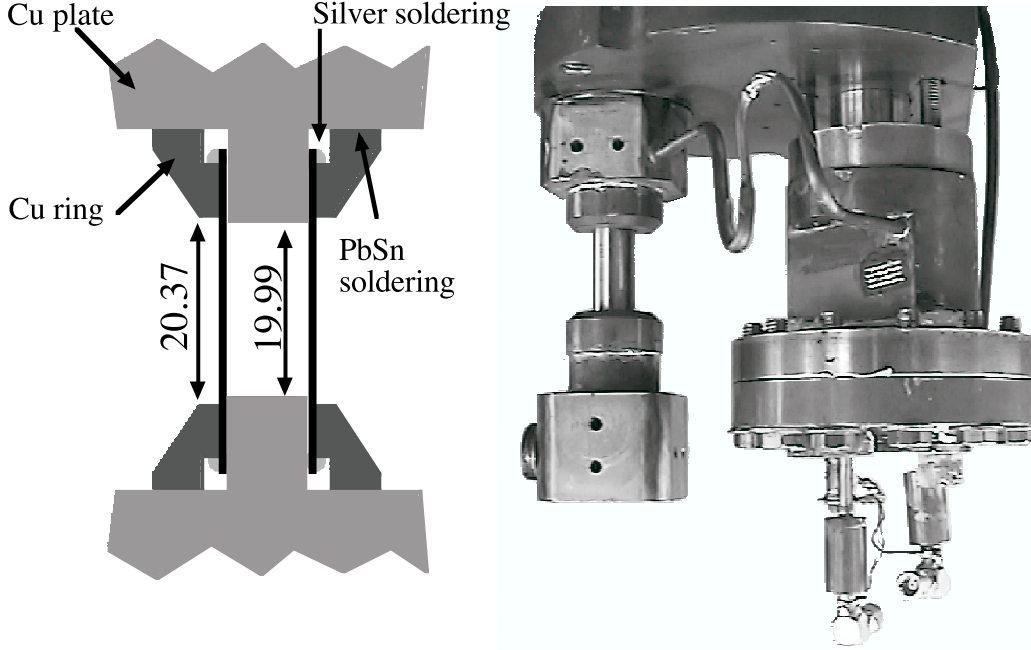


Figure 4: 4 a- The Rayleigh-Bénard cell. 4b- Photograph of the experimental set up.

going to room temperature is too large to determine the He density during the cell filling procedure with enough precision. We thus have performed an in-situ measurement using a capacitive probe located in a specific cell, in order to have a much better resolution. The density is extracted from the Clausius-Mosotti relation: $\frac{\epsilon-1}{\epsilon+2} = \frac{4\pi\zeta}{3M}\rho$, where ϵ , ρ , M , ζ are respectively the permittivity, the density, the molar mass and the polarisability of helium ($\zeta = 0.123296 \text{ cm}^3/\text{mol}$)[12].

Two capacitances are placed in a ratio bridge. The two porous frames of the "active" capacitance ($C \simeq 17.5 \text{ pF}$) are made out of printed circuits and 0.1 mm separated. This capacitance is located in the capacitive cell and totally immersed in helium. Under these conditions the mechanical dependence with pressure effects is minimized. On the inner part of each frame a circular electrode (16 mm diameter) is engraved together with a guard ring. Special attention in the design reduces differential contraction effect and parasitic capacitances : no spurious effect were detected and no temperature effects were observed. The other capacitance ($C_r = 9.4 \text{ pF}$) made out of mica, is located at 4.2 K in the calorimeter vacuum. It is the reference one.

The bridge operates at 3 kHz. The ratio between both capacitances is a direct measurement of ϵ . The density measurement range is $0 - 140 \text{ kg/m}^3$, under pressures from 0 up to 7 bars and temperatures between 4.5 and 6.5 K. Over ten days the stability is 10^{-5} ($\pm 40 \text{ g/m}^3$), that is better than 0.1% in density for Ra above $2 \cdot 10^6$. Two calibrations of the capacitance ratio at the beginning and at the end of the experiment agree within 30 g/m^3 . The signal averaged over 30 s has a resolution of 10^{-7} (less than 1 g/m^3), which can be maintained over a few hours.

In principle $k = \frac{C}{\epsilon C_r}$ should be a constant over the density range. We have achieved low and high densities calibrations. During the low pressure calibration, the cell, connected to a few litres reservoir at room temperature, is regulated at 5.432 K . For pressures lower than 1000 mbar, no condensation occurs in the filling line. In order to have stable operation conditions we restrain the low-pressure calibration below 350 mbars: a precise pressure measurement gives access to the density through ref. [13] . At high density we measured

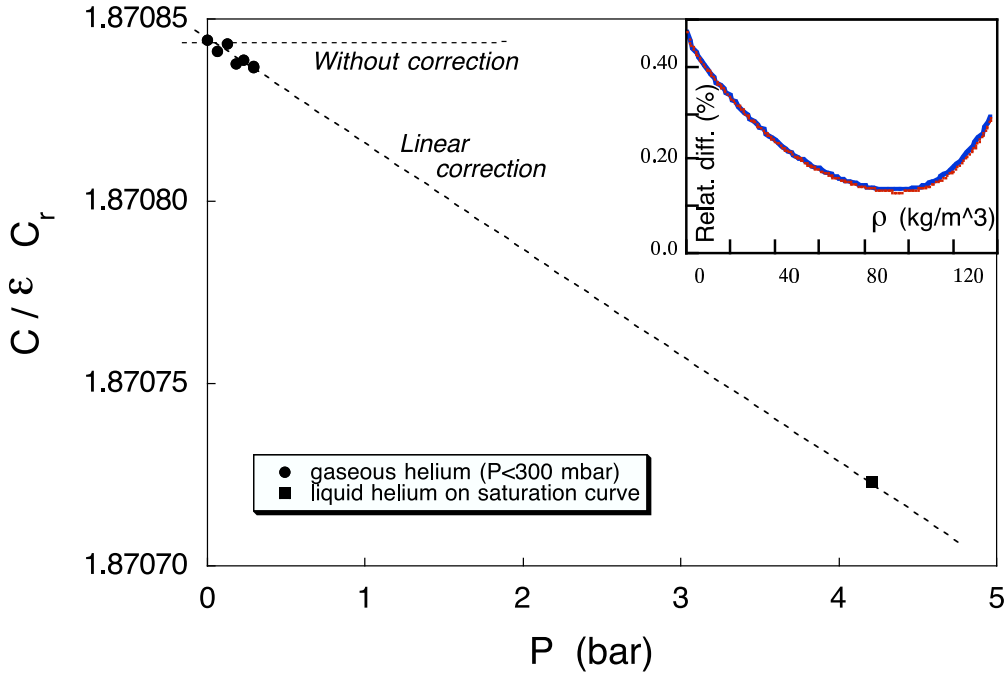


Figure 5: Calibration of the density measurement cell. Insert: Difference, in percent, between the density estimations with and without pressure correction.

the density following a procedure described below for the absolute temperature calibration (see Thermometry). For example, with $31 \mu\text{W}$ heating power applied on the bottom plate, we extract a density of 112.73 kg/m^3 from the measured boiling temperature (4.7088 K with $\Delta T = 6.5 \text{ mK}$).

The calibration results are summarized on figure 5 where $\frac{C}{\epsilon C_r}$ is plotted as a function of the pressure P . $\frac{C}{\epsilon C_r}$ varies by 6.10^{-5} over the whole range and we have assumed a linear variation versus P . Such behaviour are typical of a residual mechanical deformation. On the figure insert the difference between density with and without the linear correction is plotted versus ρ . This $\delta\rho$ is less than 0.5% and goes through a minimum at 0.15% around the critical density. In all the following we obtain the density from the linear pressure correction and we estimate the ρ uncertainty around 0.1% .

When both cells are filled and the needle valve is closed, no temperature dependence of the capacitive signal is expected. However a 0.3% tiny reproducible (on a few months scale) variation was observed as seen on figure 6. This was explained by the helium compression in the upper part of the filling line close to the needle valve in thermal contact with the main helium bath at 4.22 K . We have evidenced a linear correlation through the comparison of the total measured density and the calculated density in the capillary. The slope, plotted on the insert of figure 6 is the ratio between the total volume and the capillary dead volume : the value 23 ± 4 is in fair agreement with a less precise value extracted from a geometric determination. The ± 4 uncertainty on the volume ratio (due to the scatter of points) corresponds to a measured density uncertainty less than 0.06% on the whole densities and temperature range. It confirms by an independent way our formerly quoted 0.1% density uncertainty. Note that this capillary effect has strictly no influence on the density measurement in the cells.

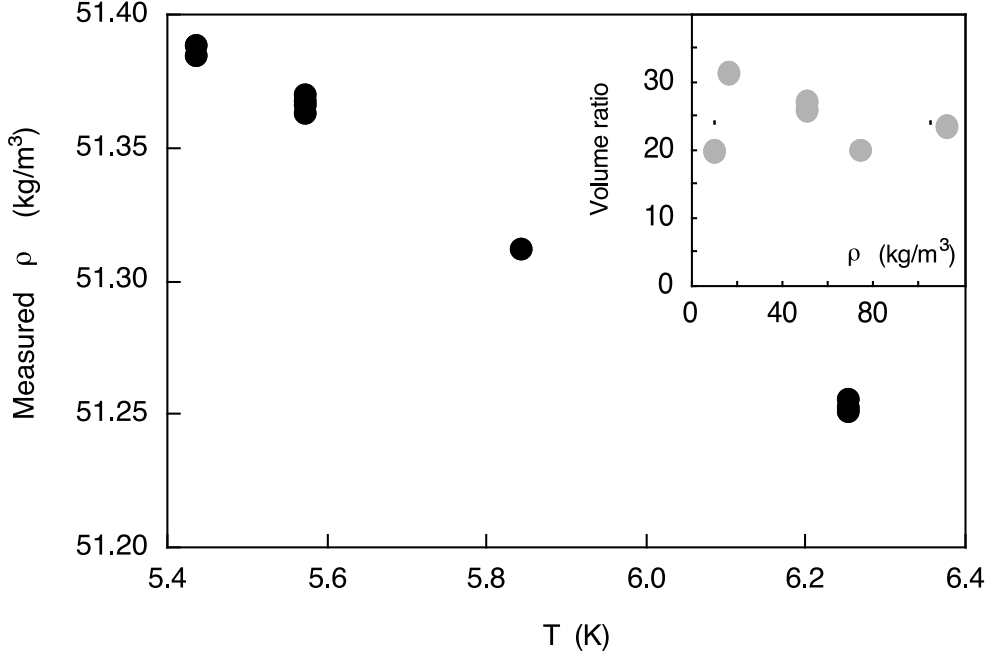


Figure 6: Measurement of the helium compression effect in the filling capillary. Insert : Measured ratio of the cells volume divided by the 4.22 K capillary volume versus density.

2.4 Thermometry

A one millikelvin uncertainty on the mean temperature gives an uncertainty up to 1% on the Ra and Nu values, in the range of temperature and density of this experiment. In order to compare the various data issued from several references[14, 15, 16, 17, 13, 18, 19, 20, 12], we use the ITS-90[21] critical temperature: $T_c = 5.1954 K$ and adjust the thermometer in-situ calibration onto that value. This calibration procedure is illustrated on figure 7 at a density of $51.5 kg/m^3$ where the condensation is expected at: $T = T_c - 47.4 mK$. We apply a small $125 \mu W$ heating power and monitor both ΔT across the Rayleigh-Bénard cell and the gas density ρ_{gas} in the capacitive cell. The temperature of the upper plate is slowly lowered. The sharp drop of ΔT and ρ_{gas} is the signature of the condensation in the cell. It is worth to note that the density measurement is more precise than the ΔT one to identify condensation and enables a $1 mK$ resolution.

3 4He properties

3.1 Thermal expansion coefficient

The reference fits of Arp and McCarty[17, 13] accounts for 4He thermodynamics properties over a wide temperature and pressure range ($0.8 - 15000 K$, $0 - 2000 MPa$) but ignores the critical divergence, which has been fitted by Kierstead[15, 16]. Unfortunately, the temperature and density validity ranges of the two fits don't overlap. Besides, extrapolation of the thermal expansion coefficient from both fits suggests up to 25% discrepancy between these fits, which is incompatible with the extrapolation uncertainty. Figure 8 illustrates

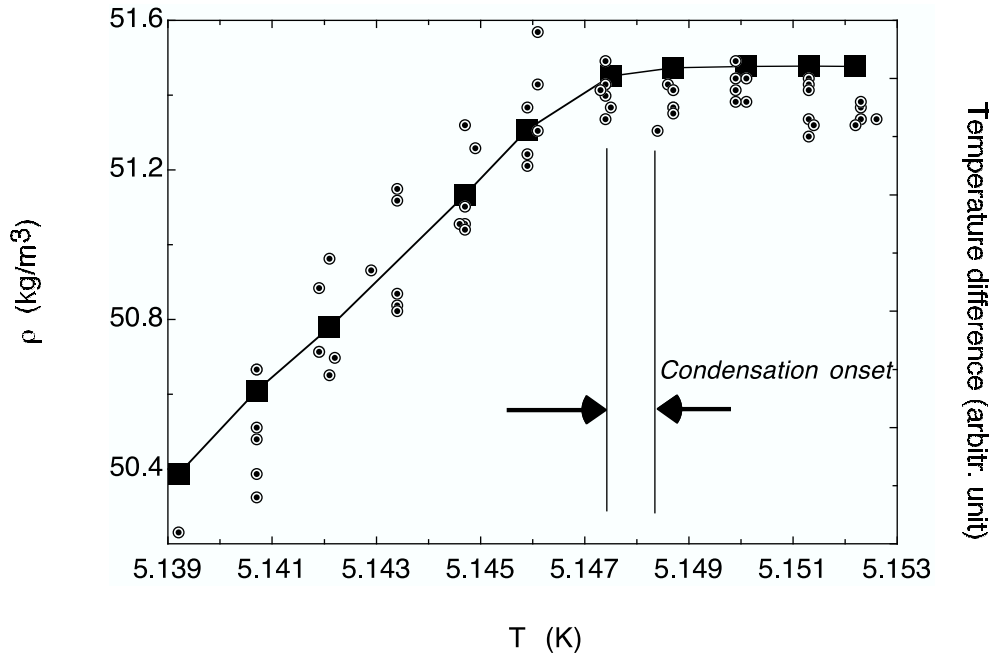


Figure 7: Full squares: Cell density versus top plate temperature around the condensation onset. Dotted circles: Plates temperature difference in arbitrary units.

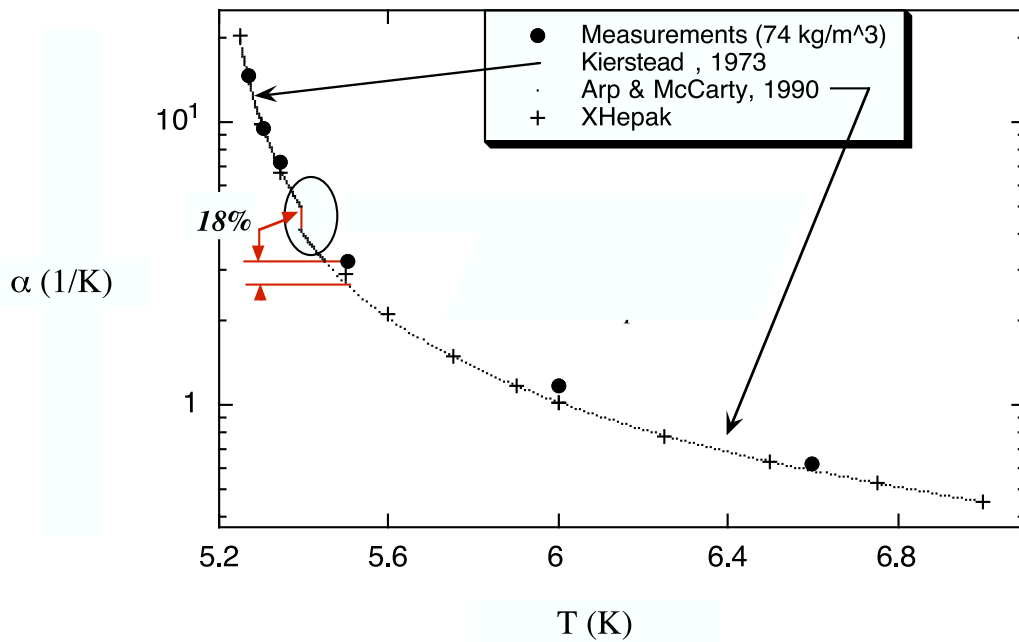


Figure 8: Comparison between the thermal expansion coefficients : present measurements (full circles) and fits (lines and pluses) at density $\rho = 74 \text{ kg/m}^3$. Kierstead[16] and McCarty and Arp[13] fits have been extrapolated in the circled area. The XHePak fit (pluses) is the commercial fitting package cited in ref. [4]

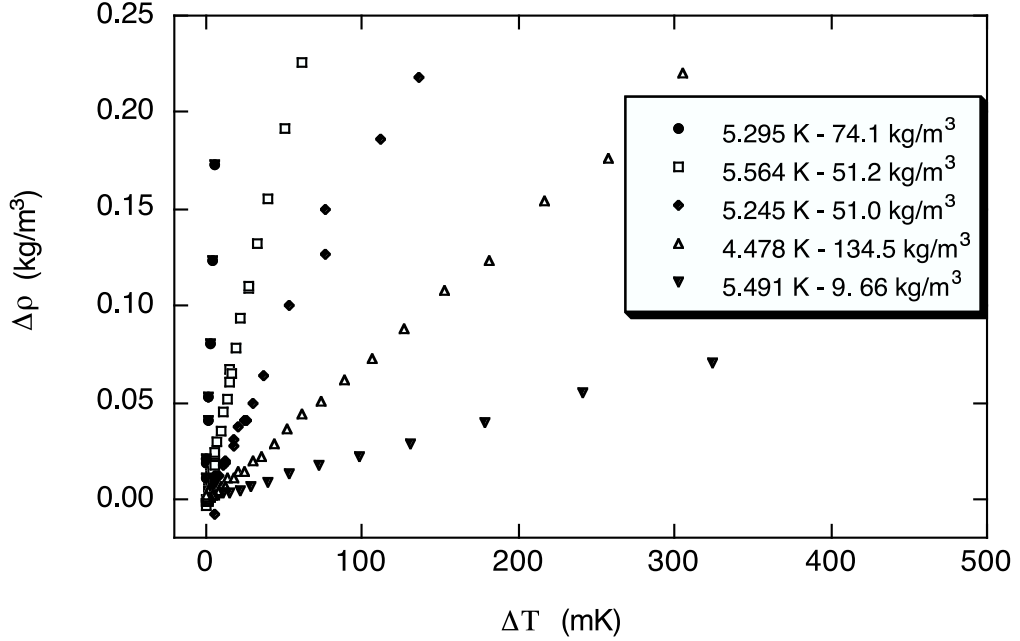


Figure 9: Capacitive measurement of the ρ increase in the capacitive cell due to the Rayleigh-Bénard cell heating versus the plates temperature difference in the convection cell.

this discrepancy for a density of $\rho = 74 \text{ kg/m}^3$.

In our experiment, the high sensitivity of the capacitive cell gives access to α , in a temperature and pressure range overlapping with both fits. The Rayleigh-Bénard cell heating increases the density in the capacitive cell. For low ΔT across the convection cell, the density variation is given by: $\delta\rho = \frac{\Delta T}{2}\rho\alpha\frac{v_2}{v_1+v_2}$, where v_1 and v_2 are the capacitive cell and Rayleigh-Bénard cell volumes respectively. The results are shown on figure 9. We extract the slope of these curves for ΔT going to 0, for given temperature and density conditions. We have also done a correction[9] to take into account the volume of the 4.2 K filling capillary below the needle valve: this correction represents a few percent at low and high densities and is smaller than 0.5% between 40 and 80 kg/m^3 . Each point corresponds to a Temperature-Density condition which fully falls into the validity range of either one of the two fits.

Determination of the geometrical coefficient $\frac{v_2}{v_1+v_2}$ is illustrated on figure 10 (the capillary volume introduces less than 1% correction on this formula and this correction is not shown here but it is taken into account in the analysis of ref. [9]). Figure 10 shows the quantity $\alpha_{est}/\frac{\alpha v_2}{v_1+v_2} = \alpha_{est}/\frac{2\delta\rho}{\rho\Delta T}$ where α_{est} is an estimated α value from the literature[17, 13, 16]. The x-axis is chosen in order to avoid the degeneracy for the data taken at same density but at various temperatures. Most of the data are compatible with the value 11.15 ± 0.25 .

As expected the data using the values from ref. [13] are very reliable far from the critical point, but they need a correction which rises up to about 20% when approaching this regime. The data from ref. [17] are in good agreement with those of ref. [13] at low density but need a correction of several percent at high density. In the critical region ref. [16] appears to give the best agreement, as illustrated in Figure 8. The various α values are summarized in Table 1.

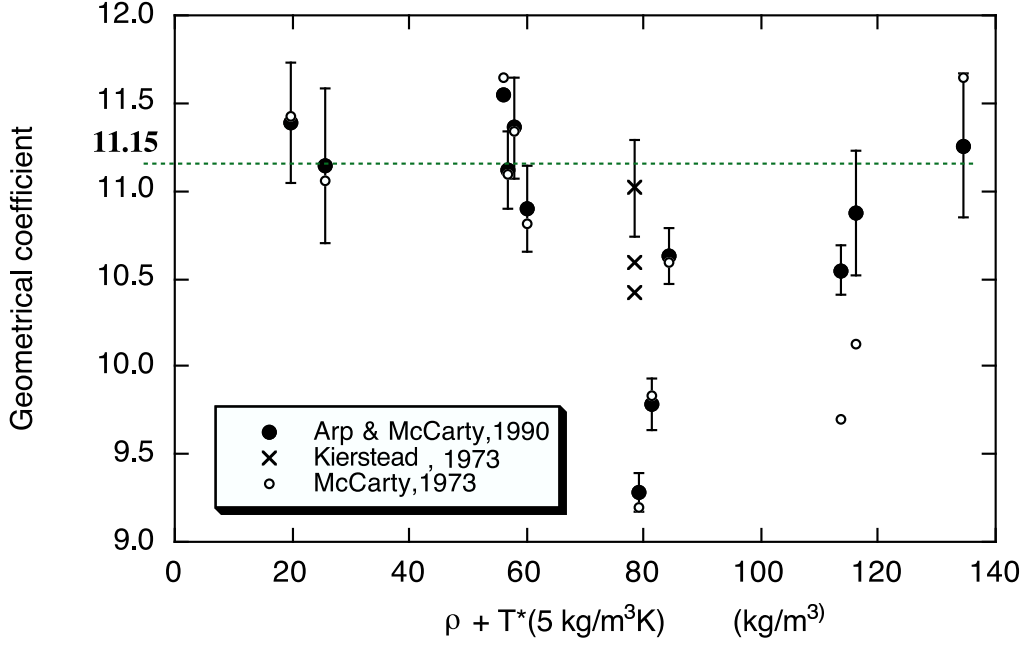


Figure 10: Geometrical coefficient (see text) versus $\rho + 5T$ for the determination of the helium expansion coefficient.

ρ (kg/m^3)	T (K)	$\alpha_{measur.}$ (K^{-1})	$\frac{\Delta\alpha_{measur.}}{\alpha_{measur.}}$ (%)	α_{MCA} (K^{-1})	$\alpha_{Kierstead}$ (K^{-1})	Measur. vs. Fit disagr. (%)
16.76	5.114	0.387	5	0.395		-2
16.70	6.270	0.266	6	0.266		0.1
51.4	5.438	2.23	3	2.311		-3.5
51.4	5.573	1.72	4	1.716		0.3
51.3	5.844	1.11	4.5	1.128		-2
51.25	6.252	0.762	4.5	0.745		2.5
74.60	5.268	14.7			14.001	5
74.31	5.305	9.48	4.5		9.3682	1
74.21	5.346	7.18	2.5		6.7188	6.5
74.06	5.503	3.21	3	2.671		18
73.87	5.999	1.170	3.5	1.027		13
73.73	6.600	0.616	3.5	0.587		5
112.3	5.260	0.349	5.5	0.340		2.5
112.6	4.725	0.478	3.5	0.453		5.5
134.6	4.490	0.1104	5.5	0.1115		-1

Table 1 : $\alpha_{measur.}$: expansion coefficient measurements, $\Delta\alpha_{measur.}$ total uncertainty on $\alpha_{measur.}$, α_{MCA} : expansion coefficient estimated with McCarty and Arp 1990 fit[13] ; $\alpha_{Kierstead}$: expansion coefficient estimated with Kierstead fit[16].

In our Rayleigh-Bénard data analysis, the α coefficient and other thermodynamical coefficients such as $(C_p - C_v)$ are obtained from the first order partial derivatives of the pressure versus temperature or density. Such a way of deriving properties ensures the self-

consistency between thermodynamics parameters. As a consequence, taking into account our measurements we have corrected the fits at their source, that is directly on the fit of $(\partial P/\partial \rho)_{T,MCA}$ of ref. [13] :

$$(\partial P/\partial \rho)_T = (\partial P/\partial \rho)_{T,MCA}[1 + (4.62 - 0.658T)[0.246 - 0.00117(\rho - 67)^2]]$$

for densities above 60 kg/m^3 and $T < 7 \text{ K}$. Below 60 kg/m^3 no correction was used. With this correction, Kierstead fit (unchanged) and Arp and McCarty fit (modified and extrapolated) reconnect.

We should mention here that C_v can't be derived from the state equation. In the zero-density region, C_v is known exactly (perfect gas) and in the critical region, it has been fitted by Moldover[14]. In between, we resorted to exact thermodynamics relation to bridge to either one of these two regions.

3.2 The transport properties : viscosity and thermal conductivity

A fit of ^4He viscosity in the range $4 - 20 \text{ K}$ and $0 - 10 \text{ MPa}$ has been proposed by Steward and Wallace[22]. In our range of parameters, the fit is an interpolation of isothermal measurements at 4, 5, 6 and 10 K conducted by these authors. Along the critical isochore, comparison with viscosity data of Kogan *et al.*[23] and Agosta *et al.*[20] shows +7% deviation at 5.2 K , -7% at 7 K . However Steward and Wallace measurements at 4, 5 and 6 K are in a few percent agreement with the literature, including the 2 references mentioned above but their data at 10 K differs significantly from the literature. It appeared that this 10 K isothermal entails a strong bias on Steward and Wallace fit down to the lower temperatures : this is consistent with a concern regarding a contamination of helium, due to a defective purifier[24]. Consequently, we derived a new interpolation between the 4, 5 and 6 K isothermals above 70 kg/m^3 and with additional data along the critical isochore[23], in the zero-density limit (ab-initio calculation of ref. [25]), and on the vapour-liquid curve[12]. The thermal conductivity has been estimated from a specially designed new fit through the data of Acton and Kellner[18, 19]. We re-computed the density data of these papers, which had been estimated with the 1973 fit of McCarty[17], even in the critical region. Our new fit agrees within $\pm 2\%$ with the published[18, 19] and unpublished[23] data of Acton and Kellner. Whenever it was possible, our convection measurements have been conducted at the same mean temperatures as the one employed by Acton and Kellner, in order to minimize interpolation errors.

4 Experimental results and analysis

The remaining of this paper presents the heat transfer measurements and their consequence. First we consider the $Nu(Ra)$ relation. Our high accuracy on Nu gives access to two new effects : the bimodality of Nu and the side-wall conductivity influence on heat transfer. We then turn to the $Nu(\text{Pr})$ dependence.

4.1 Bimodality

On figure 11 we show Nu as a function of Ra . In order to display all data with an increased vertical resolution, Nu is arbitrarily re-normalized by $Ra^{0.31}$. For comparison, we display the data at $Pr = 0.7$ and 1.1 from ref. [26]. The change in slope at $Ra \simeq 10^8 - 2 \cdot 10^8$ corresponds exactly to the soft-hard turbulent transition in 1/2 aspect ratio cell[27]. In the

soft regime, the exponent of Nu vs. Ra is close to 0.25 (interpolation over only 1.5 decade), while in the hard turbulence regime the exponent is close to 0.31, in between the $2/7$ and $1/3$ predictions of traditional theories[28]. It is interesting to note that the exponent averaged over these two regimes is close to the $2/7$. Another possible interpretation of the exponent change would be to reject the soft-hard transition picture and rather see a continuous variation of the exponent resulting from a linear combination of two power laws, although the abruptness of the exponent change, in particular at $Pr \simeq 0.95$ doesn't fully fit in this picture.

For $2.10^7 < Ra < 2.10^{10}$, points can be gathered into two subsets which differ by roughly 5 – 7% in Nu . Such a data bimodality cannot be taken into account by the uncertainties, which are twice smaller than this Nu gap, nor by a Pr dependence. Switches from one set of data to the other occur varying ΔT under quasi-constant mean temperature and density conditions (see for example $Pr \simeq 0.95$) : this definitely rules out that the bimodality would come from an improper helium property estimation in the T - ρ plane. Such a bimodality can also be seen in the large cell data from ref. [26], as shown on figure 12. A numerical simulation conducted for the same cell geometry[29] recently found that two types of large scale flow can fit the cell. This mechanism of bimodality is consistent with the invariance of the Nu gap (in log scale) observed in our data.

We cannot decide if the bimodality reveals spurious effect of the boundary conditions or a macroscopic degree of freedom of the flow with a slow dynamics. In the first hypothesis, each mode could be stabilized by the thermal inertia of boundary conditions and the switching from one mode to the other should be hysteretic. The precise anchoring mechanism didn't emerge from a first analysis of the thermal boundary conditions. The second hypothesis has drastic consequences since the very slow dynamics (at least hundreds of turn-over times) ruins -for practical reasons- the present definition of Nu : indeed a clean averaging procedure would request for a time duration incompatible with a laboratory experiment.

It is interesting to notice that this bimodality extends up to the transition to the ultimate regime for $Ra > 2.10^{11}$ as shown on figure 12. The strength of the transition to the ultimate regime, which differs from one experiment to another[3, 4], could be mode dependent, as proposed in ref. [9]. The Oregon data[4] showing no clear transition seems to belong to the upper set.

We examine now the consequences of this bimodality for Nusselt measurements in room temperature convection cells. In our set-up, the convection characteristic time h^2/κ is only a few tens of seconds, typically ten times smaller than in water at corresponding Ra . One consequence is the fast convergence of the Nu relaxation and statistics. For example, more than 330 data points are plotted on figure 11, each Nu has been averaged over typically 1 hour and after a relaxation time of a few hours. Obtaining so many data would have taken about one year and an half of continuous operation in water. Finding bimodality may have been possible in helium and not in other fluids because of this huge number of data combined with the slow dynamics of the macroscopic flow degree of freedom. Besides, the transient regime from one mode to the other is fast not only because of the short convection characteristic time but also because of the large heat diffusivity of metallic materials at cryogenic temperatures: in our plates the diffusion time is a few milliseconds and a few seconds in the side-wall. At room temperature (and above) the convection times and materials properties are far less favourable. A consequence of these differences addresses the experimental procedure of heat transfer measurement or visualization : the possibility to be in a slow transient regime should be considered. The resulting transient-regime uncertainty may be a delicate experimental issue for flow characterization studies, and a limiting factor for precise measurements, at least without new specific cell design.

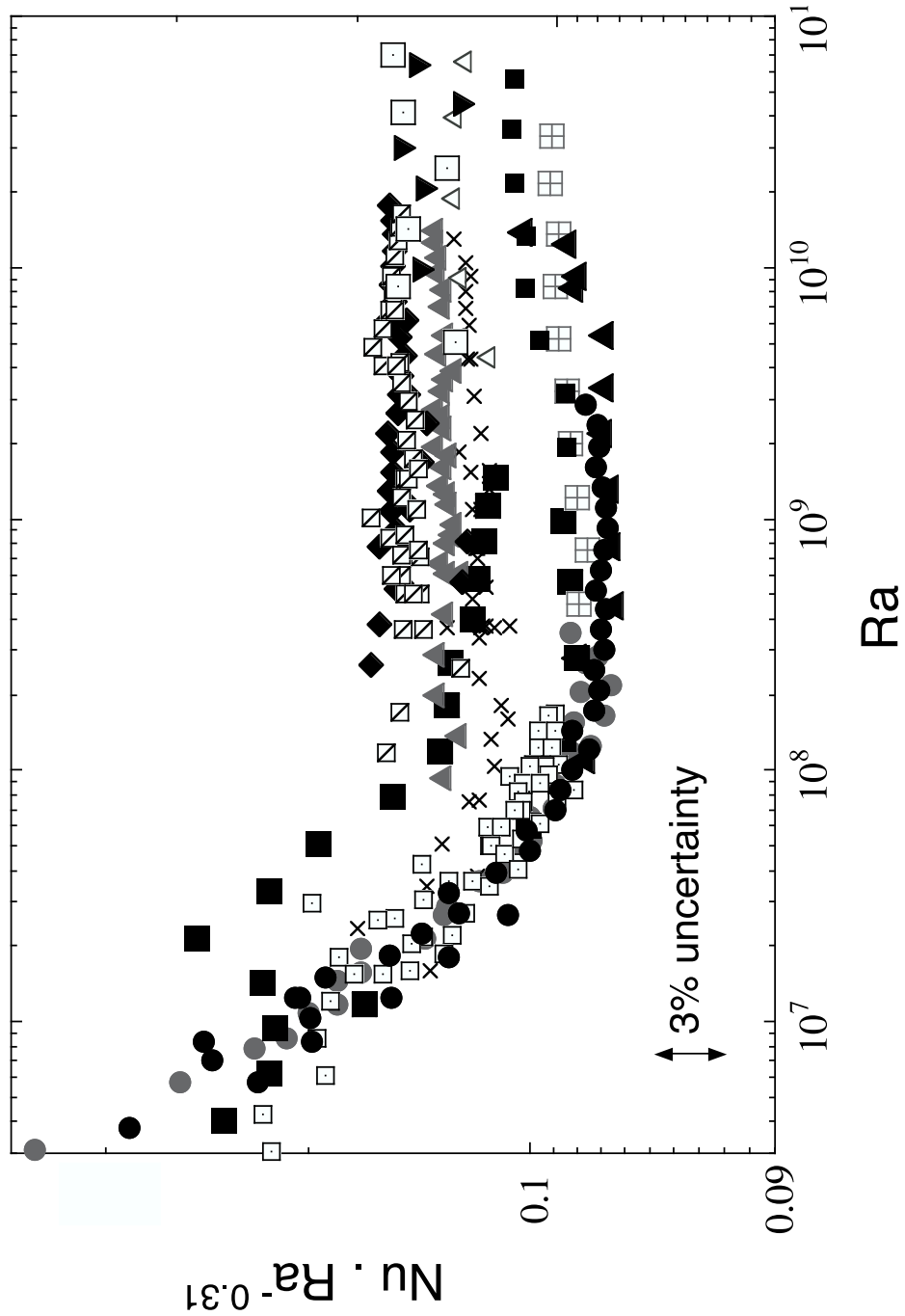


Figure 11: $NuRa^{-0.31}$ vs. Ra in the mini-cell. Black bullets: $Pr \simeq 0.73$ small framed-dot: $Pr \simeq 0.83$, grey bullets: $Pr \simeq 0.87$, large solid squares: $Pr \simeq 0.95$ empty square: $Pr \simeq 1.4$, X: $Pr \simeq 1.6 - 1.9$, grey triangles: $Pr \simeq 2.1 - 2.5$, framed-plus: $Pr \simeq 2.6 - 2.7$, framed-slash: $Pr \simeq 2.9 - 3.4$, diamonds: $Pr \simeq 3.6 - 4.3$, small solid squares: $Pr \simeq 5.8 - 6.0$, empty triangles: $Pr \simeq 10.6 - 11.3$, pointing-down triangles: $Pr \simeq 14.3 - 15.7$, For comparison, large cell[26] data are plotted with the symbols : black pointing-up-triangles: $Pr \simeq 0.7$, large framed-dot: $Pr \simeq 1.1$.

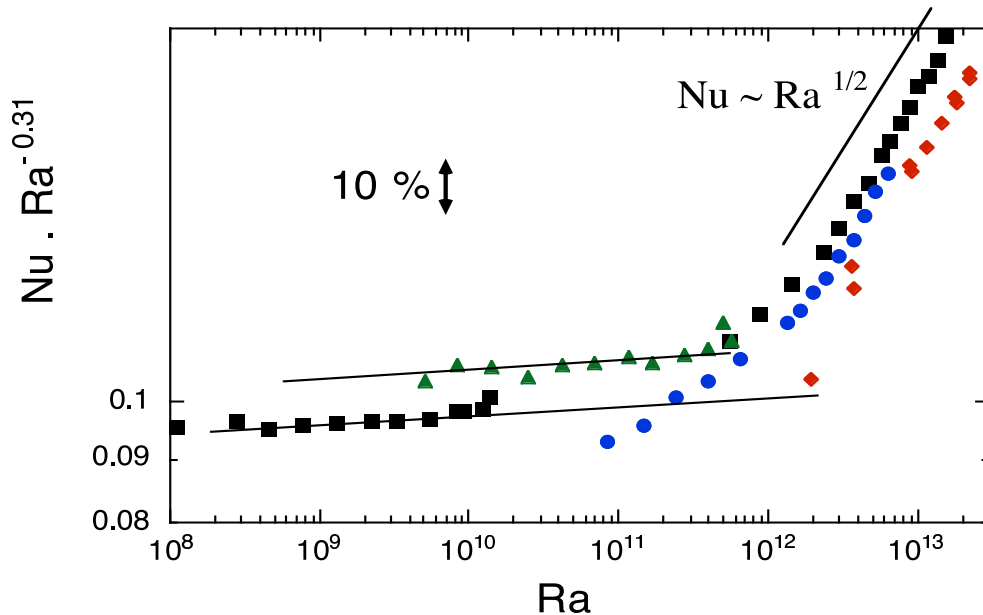


Figure 12: $NuRa^{-0.31}$ vs. Ra in a rough surface cell[26] shows bimodality up to the transition to the ultimate regime.

4.2 Side-Wall conductivity

A second outcome of this experiment was the finding of a significant and unexpected influence of the side-wall conductivity on the apparent Nusselt number : typical side wall found in the literature can indeed change Nu by more than 20%. A specific study has been conducted. We shall only summarize the results below since this work is published elsewhere[5].

The side-wall conductivity can be characterized by a dimensionless number, called the side-wall number W and defined as the ratio of the wall conductivity to the conductivity of the fluid at rest. Typical values of W for reference experiments range from nearly 0 up to 3.5. Points on figure 13 gather our heat transfer measurements (restricted to the lower "modality"). It shows that typical side-wall conductivity's can change the effective Nu by more than 20%.

We derived a closed-analytical correction formula for Nu with one adjustable parameter (continuous line of figure 13). This formula was validated versus W over more than 4 decades of Ra and later by numerical simulations. On the figure, the vertical arrows represent the correction magnitude numerically estimated by Verzicco[30]. Our correction model assumes that the effective exchange surface from the plates to the fluid is spatially extended by a side-wall surface contribution. A Nu correction based on a corrected heat flux (as proposed in [31]), rather than corrected exchange surface, gives a poorer fit on the experimental data (less of 2 decades of Ra are well corrected).

The present analysis has numerous consequences. First it explains some surprising results and discrepancies between published results, as detailed in ref. [5]. Second, the correction on Nu being Ra dependent, it changes the $Nu(Ra)$ apparent exponent, at least for $Ra < 10^{10}$. The examination of several published results indicated that the measured exponent -often close to 2/7- are significantly underestimated. Values larger than 0.3 are obtained after correction (some experiments claiming a 2/7 exponent are not subject to

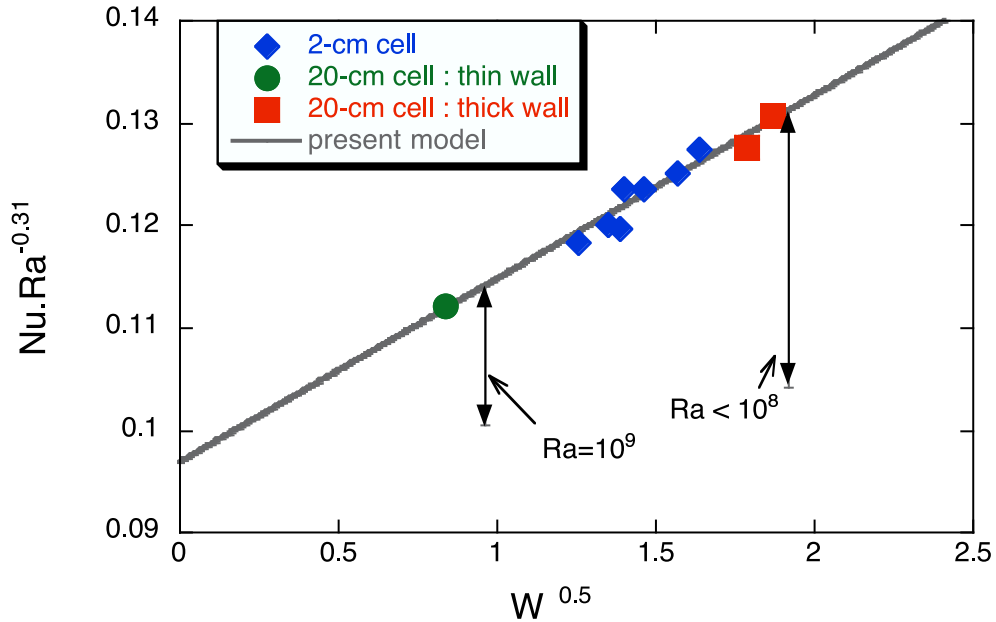


Figure 13: $Nu.Ra^{-0.31}$ vs. the square root of the side-wall number W . The symbols are experimental data obtained in the lower mode, for $10^9 < Ra < 5.10^9$ in $h = 2\text{ cm}$ and 20 cm cells. The vertical bars represent the magnitude of the side-wall correction estimated from numerical simulations by Verzicco[30]. The solid line is the present analytical model with one adjustable parameter.

side-wall correction[9]). Thirdly, it should be noted that the side-wall effect mimics a Ra dependent exponent, which could be falsely interpreted as an indication of non-power law behaviour of convection. Finally, the wall-fluid interaction is likely to introduce a new length scale in the convection problem if the wall thickness is non-uniform (flanges, large o-ring,...). Such artefact could also cause apparent non-power law behaviour.

The data presented in the rest of this paper are side-wall corrected. Note that the magnitude of the bimodality presented above is not affected by this correction.

4.3 Prandtl number dependence

Our experiment has been designed to study the influence of Prandtl number near the diffusivity cross-over $Pr \simeq 1$. We find a very small -if any- Prandtl number dependence over a 1.5 decade[35]. This dependence corresponds to an exponent smaller (in absolute value) than 0.03 in a power law picture. The 2/7 theories[36, 37] predict an exponent $-1/7 \simeq -0.14$, incompatible with our result.

A comparison with the prediction of Grossmann and Lohse[34] shows a good agreement between their predictions, (using their 5 fitting parameters adjusted to fit the data of ref. [32]) and both our data and those of ref. [33] (excepted for $Ra = 10^{10}$), as shown on figure 14. These data are for two different aspect ratio ($\Gamma = 0.5$ and 1), but once corrected for the wall effect, the influence of the aspect ratio seems poor[31]. In particular, all the set of data from the different groups suggest that the transition from the low Prandtl regime to the high Prandtl one occurs in the neighbourhood of $Pr \simeq 1$ and not 0.1 as proposed

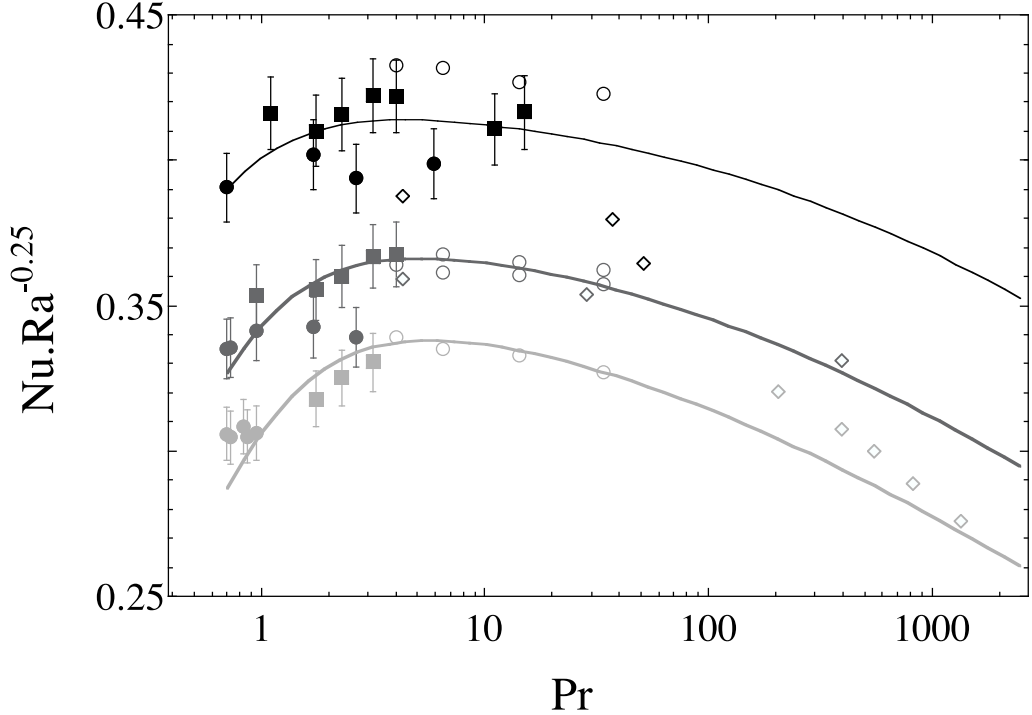


Figure 14: $Nu.Ra^{-1/4}$ vs. Pr with -from bottom to top- $Ra = 10^{8.25}$ (light gray), $Ra = 10^9$ (dark gray) and $Ra = 10^{10}$ (black). The value $Ra = 10^{8.25}$ corresponds to the beginning of the hard turbulence regime for aspect ratio $\Gamma = 0.5$. Solid circles : present data in the lower mode, Solid squares : present data in the upper mode, Open circles : data from ref. [32] ($\Gamma = 0.5$ and 1), Open diamonds : data from ref. [33] ($\Gamma = 1$). The lines are from Grossmann and Lohse[34] model with adjustable parameters tuned by these authors on the solid circles data restricted to aspect ratio $\Gamma = 1$.

by Kraichnan[28, 6].

5 Concluding remarks

The found $Nu(Ra)$ and $Nu(Pr)$ dependences are both incompatible with the 2/7 and 1/3 theories[28], at least under their present form. The Grossmann and Lohse theory[34] can account for our data but the discriminating testing of the 5 fittings parameters have to be made on a larger range of Ra and Pr numbers.

The bimodality effect indicates that the mean flow confinement has a significant influence (up to few percents) on the precise $Nu(Ra)$ dependence and this influence should hold for all aspect ratio of order 1. Since confinement effects (multi-modality, poor spatial homogeneity on boundary layers, ...) are not consider by present theories, their predicting power is indeed limited in precision. This darkens the perspective that very precise $Nu(Ra)$ measurements can discriminate between competing theories. This conclusion is reinforced by the boundary conditions influence on the global heat transfer, such as side-wall conductivity [5, 31, 30] and hole-burning effects in plates[10, 38, 11]. This underlines the importance of alternative approaches to probe the heat transfer mechanism and (in)validate theories. It also calls for a new generation of cell design with a specific attention dedicated to the

mean flow and thermal boundary conditions. For example, the influence of the large scale flow on the heat transfer suggests that large aspect ratio cell could be required to expect true power law scalings.

Acknowledgements

Acknowledgments are due to J. Niemela, J. Sommeria and R. Verzicco for fruitful discussions, and to V. Arp and H. Meyer for help in retrieving literature on helium properties.

References

- [1] D. C. Threlfall, “Free convection in low-temperature gaseous helium,” *J. Fluid. Mech.*, vol. 67 (part 1), pp. 17–28, 1975.
- [2] F. Heslot, B. Castaing, and A. Libchaber, “Transitions to turbulence in helium gas” *Phys. Rev. A*, vol. 36, no. 12, pp. 5870–73, 1987.
- [3] X. Chavanne, F. Chillà, B. Castaing, B. Hébral, B. Chabaud, and J. Chaussy, “Observation of the ultimate regime in Rayleigh-Bénard convection,” *Phys. Rev. Lett.*, vol. 79, pp. 3648, 1997.
- [4] J. Niemela, L. Skrbek, K. Sreenivasan, and R. Donnelly, “Turbulent convection at very high Rayleigh numbers,” *Nature*, vol. 404, pp. 837–840, 2000.
- [5] P.-E. Roche, B. Castaing, B. Chabaud, B. Hébral, and J. Sommeria, “Side wall effects in Rayleigh-Bénard experiments,” *Eur. Phys. J. B*, vol. 24, pp. 405–408, 2001.
- [6] R. Kraichnan, “Turbulent thermal convection at arbitrary Prandtl numbers,” *Phys. Fluids*, vol. 5, pp. 1374, 1962.
- [7] D. Tritton, *Physical Fluid Dynamics*. Clarendon Press, second ed., 1988.
- [8] X. Chavanne, *Etude du régime turbulent en convection de Rayleigh-Bénard dans l’hélium liquide ou gazeux autour de 5K*. PhD thesis, Université Joseph Fourier, Grenoble, 1997.
- [9] P.-E. Roche, *Convection thermique turbulente en cellule de Rayleigh-Bénard cryogénique*. PhD thesis, Université Joseph-Fourier, 2001.
- [10] B. Castaing, B. Chabaud, B. Hébral, X. Chavanne, O. Chanal, and P.-E. Roche, “Cryogenic turbulence experiments” in *Advances in Turbulence VIII* (C. Dopazo, ed.), Proceedings of the 8th European Turbulence Conference, (Barcelona), pp. 125–132, CIMNE Barcelona 2000.
- [11] R. Verzicco., ”Effects of plates thermal properties in turbulent thermal convection,” *Submitted to Phys. Fluids*, 2003.
- [12] R. Donnelly and C. Barenghi, “The observed properties of liquid helium at saturated vapor pressure,” *J. Phys. Chem. Ref. Data*, vol. 27, pp. 1217–74, 1998.
- [13] R. Mc Carty and V. Arp, “A new wide range equations of state for helium,” *Advances in Cryogenic Engineering (Plenum Press, New York)*, vol. 35, pp. 1465–1475, 1990. Edited by Fast R. W.

- [14] M. R. Moldover, “Scaling of the specific-heat singularity of ^4He near its critical point,” *Phys. Rev.*, vol. 182, no. 1, pp. 342–352, 1969.
- [15] H. A. Kierstead, “Pressures on the critical isochore of ^4He ,” *Phys. Rev. A*, vol. 3, pp. 329, 1971.
- [16] H. Kierstead, “PVT surface of ^4He near its critical point,” *Phys. Rev. A*, vol. 7, pp. 242251, 1973.
- [17] R. Mc Carty, “Thermodynamic properties of helium-4 from 2 to 1500 K at pressures to 10 Pa,” *J. Phys. Chem. Ref. Data*, vol. 2, pp. 923, 1973.
- [18] A. Acton and K. Kellner, “The low temperature thermal conductivity of ^4He ,” *Physica B*, vol. 90, pp. 192–204, 1977.
- [19] A. Acton and K. Kellner, “The low temperature thermal conductivity of $^4\text{He II}$ - measurements in the critical region,” *Physica B*, vol. 103, pp. 212–225, 1981.
- [20] C. Agosta, S. Wang, L. H. Cohen, and H. Meyer *J. Low Temp. Phys.*, vol. 67, pp. 237, 1987.
- [21] BIPM, “Supplementary information for the international temperature scale of 1990,” Tech. Rep., Bureau International des Poids et Mesures, Décembre 1990.
- [22] W. Steward and G. Wallace, “Helium-4 viscosity measurements 4 to 20K, 0 to 10 MN/m²,” report, NBS, Sept. 1, 1971 1971.
- [23] H. Meyer, “private communication.”
- [24] V. Arp, “private communication.”
- [25] R. A. Aziz, A. R. Janzen, and M. R. Moldover, “Ab initio calculations for helium: a standard for transport property measurements,” *Phys. Rev. Lett.*, vol. 74, no. 9, pp. 1586–1589, 1995.
- [26] P.-E. Roche, B. Castaing, B. Chabaud, and B. Hébral, “Observation of the 1/2 power law in Rayleigh-Bénard convection,” *Phys. Rev. E*, vol. 63, pp. 045303(R), 2001.
- [27] X. Wu, *Along a road to developed turbulence : free thermal convection in low temperature Helium gas*. PhD thesis, University of Chicago, 1991.
- [28] E. Siggia, “High Rayleigh number convection,” *Annual Review of Fluid Mechanics*, vol. 26, pp. 137–168, 1994.
- [29] R. Verzicco and R. Camussi, “Numerical experiments on strongly turbulent thermal convection in a slender cylindrical cell,” *J. Fluid Mech.*, vol. 477, pp. 19–49, 2003.
- [30] R. Verzicco, “Side wall finite conductivity effects in confined turbulent thermal convection,” *J. Fluid Mech.*, vol. 473, pp. 201–210, 2002.
- [31] G. Ahlers, “Effect of sidewall conductance on heat-transport measurements for turbulent Rayleigh-Bénard convection,” *Phys. Rev. E*, vol. 63, pp. 015303(R), 2001.
- [32] G. Ahlers and X. Xu, “Prandtl-number dependence of heat transport in turbulent Rayleigh-Bénard convection,” *Phys. Rev. Lett.*, vol. 86, pp. 3320, 2001.
- [33] K. Xia, S. Lam, and S. Zhou, “Heat-flux measurement in high-Prandtl-number turbulent Rayleigh-Bénard convection,” *Phys. Rev. Lett.*, vol. 88, pp. 064501, 2002.

- [34] S. Grossmann and D. Lohse, “Thermal convection for large Prandtl numbers,” *Phys. Rev. Lett.*, vol. 86, pp. 3316, 2001.
- [35] P.-E. Roche, B. Castaing, B. Chabaud, and B. Hébral, “Prandtl and Rayleigh numbers dependences in Rayleigh-Bénard convection,” *Europhys. Lett.*, vol. 58, pp. 693–698, 2002.
- [36] B. Castaing, G. Gunaratne, F. Heslot, L. Kadanoff, A. Libchaber, S. Thomae, X. Wu, S. Zaleski, and G. Zanetti, “Scaling of hard thermal turbulence in Rayleigh-Bénard convection,” *J. Fluid Mech.*, vol. 24, pp. 137–167, 1989.
- [37] B. I. Shraiman and E. D. Siggia, “Heat transport in high-Rayleigh-number convection,” *Phys. Rev. A*, vol. 42, pp. 3650–53, 1990.
- [38] S. Chaumat, Castaing B., and Chilla F., ”Rayleigh-Bénard cells: influence of the plate properties,” in *Advances in Turbulence IX* (I. P. Castro and P. E. Hancock, ed.) Proceedings of the 9th European Turbulence Conference, (Southampton, UK),pp. 159–162, CIMNE Barcelona 2002.